Article:
Ochs, O., Hocke, M., Spitzer, S. et al. (3 more authors) (2020) Origin of solvent-induced polymorphism in self-assembly of trimesic acid monolayers at solid-liquid interfaces. Chemistry of Materials. ISSN 0897-4756

https://doi.org/10.1021/acs.chemmater.0c00827

Origin of Solvent-Induced Polymorphism in Self-Assembly of Trimesic Acid Monolayers at Solid-Liquid Interfaces

Oliver Ochs[†], *Manuela Hocke*[†], *Saskia Spitzer*[†], *Wolfgang M. Heckl*[†], *Natalia Martsinovich*[‡], *and Markus Lackinger*[†]*

†Department of Physics, Technische Universität München, James-Franck-Str. 1, 85748 Garching, Germany; Deutsches Museum, Museumsinsel 1, 80538 Munich, Germany;

‡Department of Chemistry, University of Sheffield, Sheffield S3 7HF, UK;

ABSTRACT

Encoding information in the chemical structure of tectons is the pivotal strategy in self-assembly for the realization of targeted supramolecular structures. However, frequently observed polymorphism in supramolecular monolayers provides experimental evidence for a decisive additional influence of environmental parameters, such as solute concentration or type of solvent, on structure selection. While concentration-induced polymorphism is comparatively well understood, the thermodynamical and molecular origins of solvent-induced polymorphism remain elusive. To shed light on this fundamental aspect of self-assembly, we explore the solvent-induced polymorphism of trimesic acid (TMA) monolayers on graphite as prototypical

example. Using the homologous series of fatty acids as solvents, TMA self-assembles into the anticipated chickenwire polymorph for longer chain fatty acids, whereas the more densely packed, but still porous flower polymorph emerges in shorter chain fatty acids. According to our initial working hypothesis, the origin of this solvent-induced polymorphism lies in a solvent-dependence of the free energy gain. Utilizing an adapted Born-Haber cycle constructed from measured TMA sublimation and dissolution enthalpies as well as Density Functional Theory calculated monolayer binding energies, we quantitatively assessed the self-assembly thermodynamics of both polymorphs in hexanoic, heptanoic, and nonanoic acid. Yet, in contrast to the experimental findings, these results suggest superior thermodynamical stability of the chickenwire polymorph in all solvents. On the other hand, additional experiments comprising variable temperature Scanning Tunneling Microscopy corroborate that the flower polymorph is thermodynamically most stable in hexanoic acid. To resolve this apparent contradiction, we propose a thermodynamical stabilization of the flower polymorph in hexanoic acid through the stereochemically specific co-adsorption of shape-matched solvent molecules in its unique smaller elongated pores. This alternative explanation gains further support from experiments with side-substituted hexanoic acid solvents. Combination of a quantitative thermodynamic analysis and studies with systematic variations of the solvent's molecular structure holds great promise to enhance the understanding of thus far underexplored solvent effects.

INTRODUCTION

The power of molecular self-assembly lies in its potential to realize targeted supramolecular structures by encoding their blueprints in the chemical structure of the tectons through the stereochemical arrangement of functional groups for intermolecular binding. The reliable expression of specific intermolecular binding motifs either facilitates structure prediction, or provides the basis for tailoring tectons for targeted structures. Carboxylic acid moieties are a prominent example thereof as they predominantly form, according to graph-set notation,[1] $R_2^2(8)$ cyclic double hydrogen bonds (H-bonds). Exclusive and full expression of this intermolecular binding motif, for instance in C_{3v} symmetric tricarboxylic acids, necessarily results in honeycomb networks.[2] Supramolecular monolayers at liquid-solid interfaces constitute an ideal study object for fundamental research, not at least because structures are readily resolved by Scanning Tunneling Microscopy (STM).[3] Moreover, due to their vast variability in structure, composition, and chemistry, as well as the straightforward preparation, interfacial supramolecular monolayers bear great potential for applications in surface patterning and functionalization.

Frequently observed polymorphism in supramolecular monolayers, however, clearly indicates that structures are not predetermined by the tecton's chemical structure, but rather reveals an additional, occasionally decisive influence of environmental parameters such as type of solvent, solute concentration, surface, and temperature.[4-19] It is by no means obvious whether the observed polymorphism originates from kinetic effects or is governed by equilibrium thermodynamics.[20-21] For the concentration-induced polymorphism, the observation of more densely packed polymorphs for higher solute concentrations seems to hold universally, and is consistently explained by a generic thermodynamic origin: higher solute concentrations are

associated with enhanced chemical potential; Thereby more densely packed structures gain thermodynamic stability, essentially due to the reduced entropy cost of self-assembly. This readily explains why even polymorphs with energetically inferior binding motifs can become thermodynamically selected.[22] While the physicochemical effect of solute concentration on polymorph selection is arguably best understood, the role of further environmental parameters remains elusive. Among those, the type of solvent is crucially important, because solvents can have a pronounced affect, but are chosen on a largely empirical basis. Often various solvents are tediously tested until self-assembly of stable monolayers is eventually accomplished. For a more insightful approach, it is desirable to gain fundamental knowledge either on thermodynamical grounds or even more profoundly at the molecular level on why and how specific solvents stabilize distinct polymorphs. As a widely studied model system we explore the solvent-induced polymorphism of trimesic acid (benzene-1,3,5-tricarboxylic acid, TMA) monolayers. This small, highly symmetric, and conformationally rigid tecton gives rise to an astonishingly large number of distinct structures and intriguing observations.[23-41] Here we concentrate on the solvent-induced polymorphism observed for the homologous series of fatty acid solvents on graphite,[26] as the first reported case of a phenomenon that turned out to be common.[4-14] Although our original publication dates back to the year 2005, no detailed account on the origin of this paradigmatic finding has been yet provided.

Results and Discussion

Using the homologous series of unbranched fatty acids as solvents, two hexagonal TMA monolayer polymorphs termed flower and chickenwire are observed at the interface to graphite, whereby the former polymorph self-assembles in shorter chain fatty acids up to hexanoic acid (6A) and the latter polymorph in longer chain fatty acids from heptanoic acid (7A) onward.[26]

STM images alongside with corresponding Density Functional Theory (DFT) optimized structures of both polymorphs on graphite are presented in Figure 1. The chickenwire polymorph exclusively features $R_2^2(8)$ cyclic double H-bonds bonds between all carboxylic acid groups, resulting in a hexagonal structure with two TMA per unit cell and a=b=(1.65 ± 0.05) nm. In the flower polymorph, one out of the three carboxylic acid groups of each TMA is involved in $R_3^3(12)$ cyclic H-bonds, resulting likewise in a hexagonal structure, yet with six molecules per unit cell and a=b=(2.60 ± 0.05) nm. Both polymorphs feature H-bonded supramolecular rings comprised of six TMA as secondary building blocks that delimit circular pores with a diameter of ~1.0 nm (green circles in Figure 1). In the chickenwire polymorph these hexameric rings are interwoven, that is each TMA simultaneously belongs to three adjacent rings, whereas in the flower polymorph these rings are hexagonally close packed and each TMA uniquely belongs to one ring. This packing results in smaller elongated pores between the edges of the hexameric rings that are unique for the flower polymorph (orange ovals in Figure 1). In both polymorphs all TMA are equivalent with respect to their intermolecular binding. Remarkably, other TMA polymorphs are not known at liquid-solid interfaces, with the exception of heavily sonicated solutions.[33] But in this case structure formation is not well understood, and its reasons may as well lay beyond equilibrium thermodynamics. A possible explanation is provided under the premise that at least one carboxylic acid group of each TMA must form $R_2^2(8)$ H-bonds. If alternatively only $R_3^3(12)$ H-bonds are allowed, the only remaining fully H-bonded polymorphs are chickenwire and flower.

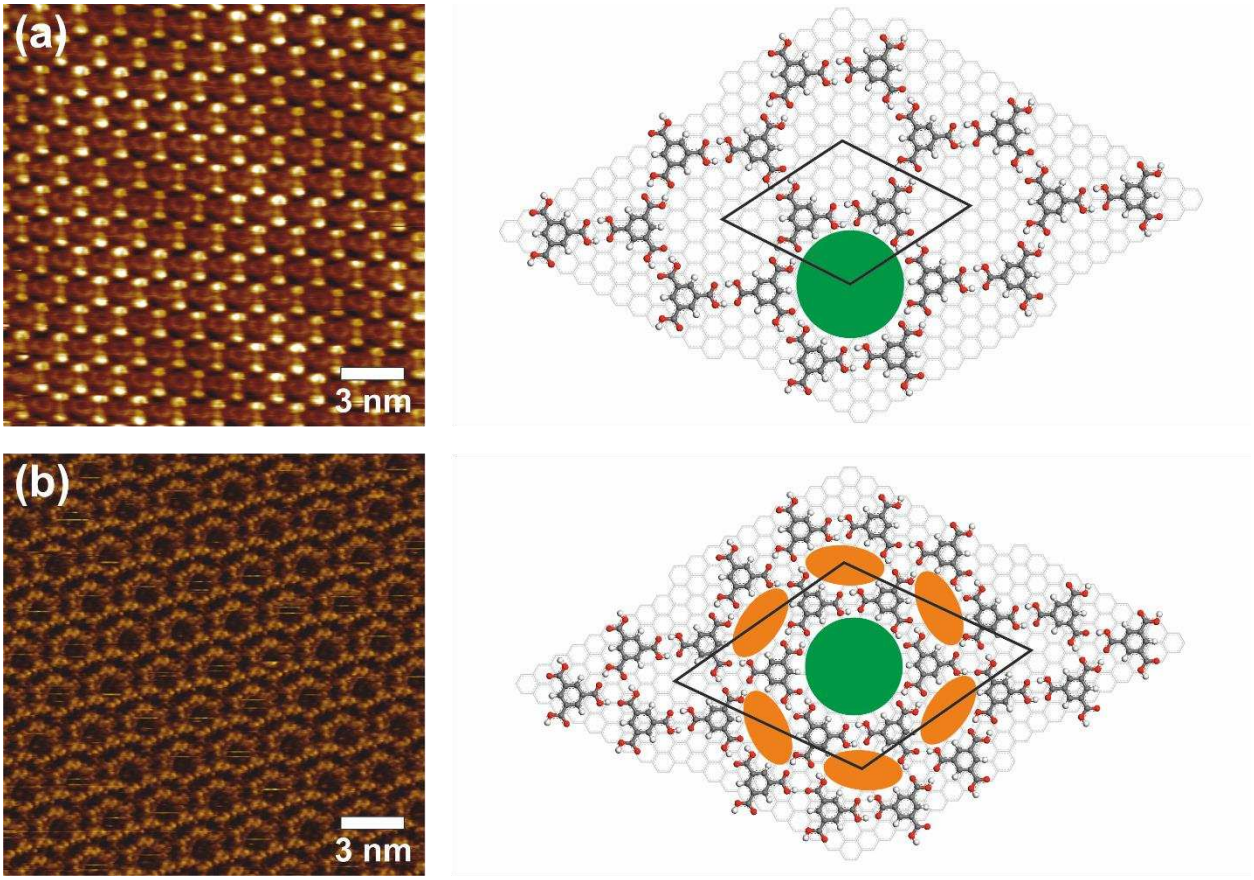

Figure 1. STM images of TMA (a) chickenwire and (b) flower polymorph on graphite(0001) acquired in saturated 9A and 6A solution, respectively. On the right hand side, the corresponding DFT-optimized structures are shown (for clarity only the topmost graphite layer is depicted, while the calculations were carried out on two layer slabs). The hexagonal unit cells are outlined by black lines. Green circles highlight the ~1 nm large circular pores that are common to both polymorphs, while orange ovals highlight the smaller elongated pores that are unique for the flower polymorph. (sample voltages and current setpoints: (a) 510 mV, 41 pA; (b) 1.01 V, 84 pA).

Quantitative thermodynamics

Scheme 1. Born-Haber cycle for the indirect determination of the enthalpic driving force $\Delta H_{sol-mono}$ of monolayer self-assembly on solid surfaces from solution.

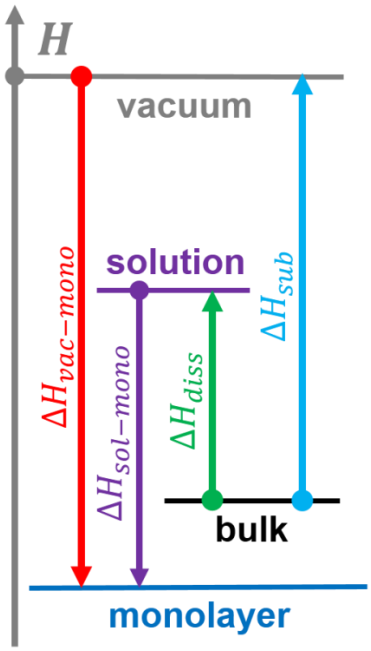

According to the fundamental theoretical study by Conti and Cecchini, the polymorph that results in the lowest (most negative) free energy gain per unit area $\Delta g = \frac{\Delta G}{A} = \Delta h - T \cdot \Delta s$ is thermodynamically most stable at liquid-solid interfaces.[42] This work forms the foundation for our initial working hypothesis: the origin of the TMA solvent-induced polymorphism lies in a distinct solvent and polymorph dependence of Δg (primary solvent effect). Consequently, Δg would be lower (more negative) for the flower than for the chickenwire polymorph in 6A, whereas Δg would be lower for the chickenwire than for the flower polymorph in 7A and longer chain fatty acids. Thereby, solvent influences on either the enthalpy gain or the entropy cost for self-assembling TMA from solution are similarly conceivable, and could both give rise to higher

thermodynamic stability of the flower polymorph in 6A. An accurate quantification of solvent effects on the enthalpy gain is of primary importance, while any assessment solely based on monolayer binding energies with respect to vacuum is insufficient. Yet, obtaining accurate values for the monolayer enthalpy with respect to solution is challenging for both experiment and theory. As a first step toward quantifying the solvent influence, we proposed a Born-Haber cycle for self-assembly from solution,[43] as illustrated in Scheme 1. The enthalpy difference between solution and monolayer ($\Delta H_{sol-mono}$) is indirectly determined from the sublimation enthalpy (ΔH_{sub}), the monolayer binding enthalpy with respect to vacuum ($\Delta H_{vac-mono}$), and the dissolution enthalpy (ΔH_{diss}):

$$\Delta H_{sol-mono} = -\Delta H_{diss} + \Delta H_{sub} + \Delta H_{vac-mono}$$

Within this approach the solvent dependence is contained in ΔH_{diss}, hence measurements for different solvents are the key for unveiling the solvent-dependence of $\Delta H_{sol-mono}$ as a possible thermodynamic origin of solvent-induced polymorphism. For a complete assessment, a non-negligible dewetting enthalpy ΔH_{dewet} has to be included that accounts for differences in interfacial energy, when the graphite-solution is replaced by the monolayer-solution interface.[43] For the moment we ignore ΔH_{dewet} , but will discuss its influence later.

Effusion experiments in high vacuum yield $\Delta H_{sub} = 154\ \frac{kJ}{mol}$ for TMA (cf. Supporting Information) in perfect agreement with literature values.[44] $\Delta H_{vac-mono}$ was obtained from DFT calculations. Detailed analysis of the Moiré pattern inherent in the chickenwire polymorph revealed its incommensurability with respect to graphite.[39] To nevertheless facilitate periodic boundary conditions, we used a quadrupled unit cell based on a commensurate $\begin{pmatrix} 14 & 1 \\ -1 & 13 \end{pmatrix}$ superstructure containing eight TMA. Thereby the tensile strain in comparison to a free-standing

monolayer could be kept below 1%, and the resulting angle between TMA and graphite lattice of 3.9° lies well within the experimental range. For the flower polymorph we used a commensurate $\begin{pmatrix} 11 & 1 \\ -1 & 10 \end{pmatrix}$ superstructure for a single unit cell containing six TMA, in accord with experimental lattice parameters (cf. Supporting Information). DFT calculations result in $\Delta H_{vac-mono}$ per TMA of $-180.3\ \frac{kJ}{mol}$ for the chickenwire and $-173.0\ \frac{kJ}{mol}$ for the flower polymorph in agreement with reported values.[37, 42, 45] The corresponding intermolecular binding energies, that is without TMA-graphite interactions, amount to $-91.9\ \frac{kJ}{mol}$ and $-80.6\ \frac{kJ}{mol}$ per TMA for chickenwire and flower polymorph, respectively. An enthalpic preference for the chickenwire polymorph was expected and originates in the diminished strength of $R_3^3(12)$ as compared to $R_2^2(8)$ H-bonds.[46] Interestingly, the chickenwire polymorph features a slightly weaker adsorption energy per TMA (unit cell averaged) of $-88.4\ \frac{kJ}{mol}$ as compared to $-92.4\ \frac{kJ}{mol}$ for the flower polymorph, suggesting more favorable TMA adsorption sites in the flower polymorph, as plausibly expected for a commensurate superstructure.

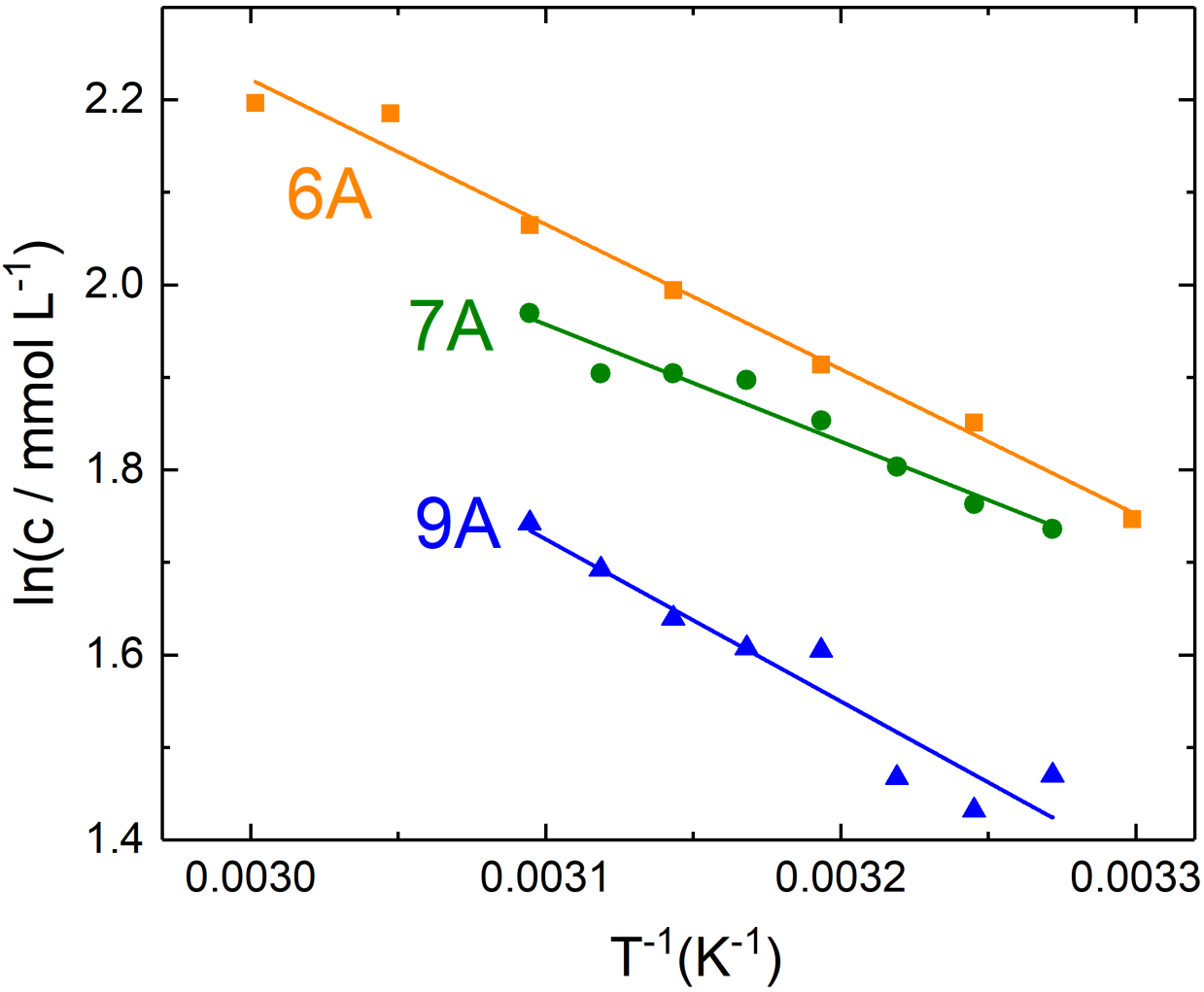

Figure 2. Van't Hoff plots of the temperature-dependence of TMA solubility in 6A (orange squares), 7A (green circles), and 9A (blue triangles) as determined from UV-Vis absorption spectroscopy. Symbols represent individual measurements, whereas the lines represent linear fits. The negative slope corresponds to the dissolution enthalpy ΔH_{diss} in the respective solvent, whereas the intercepts correspond to the standard dissolution entropies ΔS^0_{diss} (both in units of the universal gas constant R).

ΔH_{diss} were experimentally determined in 6A, 7A, and nonanoic acid (9A) through measuring the temperature-dependence of TMA solubility by UV-Vis absorption spectroscopy (cf.

Supporting Information for full data sets). Van't Hoff plots for all three solvents are summarized in Figure 2. The (negative) slopes correspond to ΔH_{diss}, while the intercepts correspond to the standard dissolution entropy ΔS^0_{diss}. Fitting the data with straight lines results in $\Delta H_{diss}(6A) = +13.0\,\frac{kJ}{mol}$, $\Delta H_{diss}(7A) = +10.5\,\frac{kJ}{mol}$, and $\Delta H_{diss}(9A) = +14.6\,\frac{kJ}{mol}$. These values are rather similar and do not show a clear trend, but appear surprisingly small. Dissolving TMA could be expected to be highly endothermic, because of the strong H-bonded networks in the bulk crystal, as reflected by the large ΔH_{sub}. Yet, the small ΔH_{diss} can readily be explained by a superb stabilization of TMA solutes in solution through solvation by H-bonding with fatty acid solvent molecules. Thereby the broken H-bonds from the bulk crystal are retained and their contribution to ΔH_{diss} becomes effectively neutralized.[43, 47] As evident from Scheme 1, for a given molecule, hence a fixed ΔH_{sub}, a larger (more endothermic) ΔH_{diss} leads to a higher $\Delta H_{sol-mono}$, that is a larger enthalpic driving force for adsorption from solution. For a meaningful comparison of competing polymorphs, however, molecular packing densities have to be taken into account. Therefore we evaluated the enthalpy gain per unit area $\Delta h = \frac{\Delta H_{sol-mono}}{A_{molecule}}$. Thereby $A_{molecule}$ is the average area per TMA in the monolayers and was derived from the experimental lattice parameters. Results for both TMA polymorphs in all three solvents are summarized in Table 1, and indicate an enthalpic preference for the chickenwire polymorph in all three solvents. Yet, the differences in Δh are comparatively small, and possibly lie below the experimental error.

Table 1. Experimental lattice parameters $a = b$ of both hexagonal structures, resulting area per molecule $A_{molecule}$, and enthalpy gain per unit area Δh for both polymorphs in all three solvent as estimated from the Born-Haber cycle.

	chickenwire	*flower*

$a\ (nm)$	*1.65*	*2.60*
$A_{molecule}\ (nm^2)$	*1.18*	*0.976*
$\Delta h(6A)\ (\frac{kJ}{nm^2})$	*-33.4*	*-32.8*
$\Delta h(7A)\ (\frac{kJ}{nm^2})$	*-31.2*	*-30.3*
$\Delta h(9A)\ (\frac{kJ}{nm^2})$	*-34.7*	*-34.4*

On the other hand, self-assembly of more densely packed polymorphs is also associated with higher entropy cost. Hence, it is not sufficient to solely consider the enthalpy gain, but the entropy cost similarly has to be taken into account. Yet, its accurate quantification is even more challenging and currently remains beyond reach. Hence, we propose using the absolute values of ΔS^0_{diss}, that reflects the entropy difference between TMA in solution and in the bulk crystal, as relative measure for the solvent-dependence of the entropy cost. This approach implies comparable entropies of TMA in the monolayer and in the bulk crystal as justified by the essentially similar H-bonding environment. Even though minor differences could arise from vibrational entropy, it is important to state that the solvent-dependence is captured. Standard dissolution entropies ΔS^0_{diss} correspond to the intercepts of the Van't Hoff plots in Figure 2, resulting in $\Delta S^0_{diss}(6A) = 57.5\ \frac{J}{mol \cdot K}$, $\Delta S^0_{diss}(7A) = 48.9\ \frac{J}{mol \cdot K}$, and $\Delta S^0_{diss}(9A) = 59.5\ \frac{J}{mol \cdot K}$. The higher value for 6A than for 7A not only explains the higher TMA solubility, but also indicates a larger entropy cost per molecule for TMA self-assembly from 6A solutions. But again it is the entropy cost per unit area $\Delta s = \frac{\Delta S}{A_{molecule}}$ that is relevant for monolayer self-assembly. $A_{molecule}$ for the chickenwire polymorph is about 20% larger than for the more densely packed flower polymorph (cf. Table 1). Consequently, for equal entropy cost per molecule ΔS, the entropy cost

per unit area Δs is about 20% larger for the flower than for the chickenwire polymorph. Although the differences in Δh are relatively small between both polymorphs, the significantly larger Δs of the flower polymorph results in a pronounced thermodynamical preference of the chickenwire polymorph in all solvents. In particular, 6A, which features an almost 20% larger ΔS than 7A, while the Δh values are comparable, would be a less likely solvent to thermodynamically stabilize the flower polymorph through a primary solvent effect.

Lastly, we qualitatively discuss the influence of the experimentally hardly accessible dewetting enthalpy ΔH_{dewet} on TMA polymorph selection. Our previous molecular mechanics calculations suggested that the solution-monolayer interface is energetically less favourable than the solvent-graphite interface,[43] in particular for alkanoic solvents that adsorb relatively strongly on graphite. Consequently, the enthalpy contribution from dewetting should be endothermic. Moreover, the chickenwire polymorph exposes a larger area fraction of the underlying graphite to solution due to its smaller packing density, i.e. higher porosity (cf. Table 1). Based on these considerations, we propose that the endothermic ΔH_{dewet} should be larger for the flower polymorph, further contributing to its inferior thermodynamic stability.

Thermodynamics *versus* Kinetics

In all experiments with 6A as solvent, exclusively the flower polymorph was observed despite its putative thermodynamic instability against the chickenwire polymorph. This raises the question of a possible kinetic stabilization. Several studies unambiguously demonstrate kinetic trapping of supramolecular monolayers at liquid-solid interfaces,[48-52] implying that the perception of an effective dynamic equilibrium does not necessarily hold true. The most common way of experimentally addressing this crucial point are additional thermal treatments to promote

attainment of the thermodynamic equilibrium.[48, 51, 53] Commonly, samples are *ex-situ* heated and subsequently characterized by STM at room temperature. Yet *in-situ* experiments with STM imaging at elevated temperatures provide unique and detailed molecular level insights by directly assessing the sample state at the respective temperature.[16-17, 54] To conduct these experiments with the comparatively volatile 6A solvent, we employed our recently developed Immersion-STM (I-STM).[55] This instrument was designed for long-term experiments at liquid-solid interfaces at elevated temperatures with unprecedentedly low drift and high resolution, while solvent evaporation is fully eliminated by a hermetic enclosure.

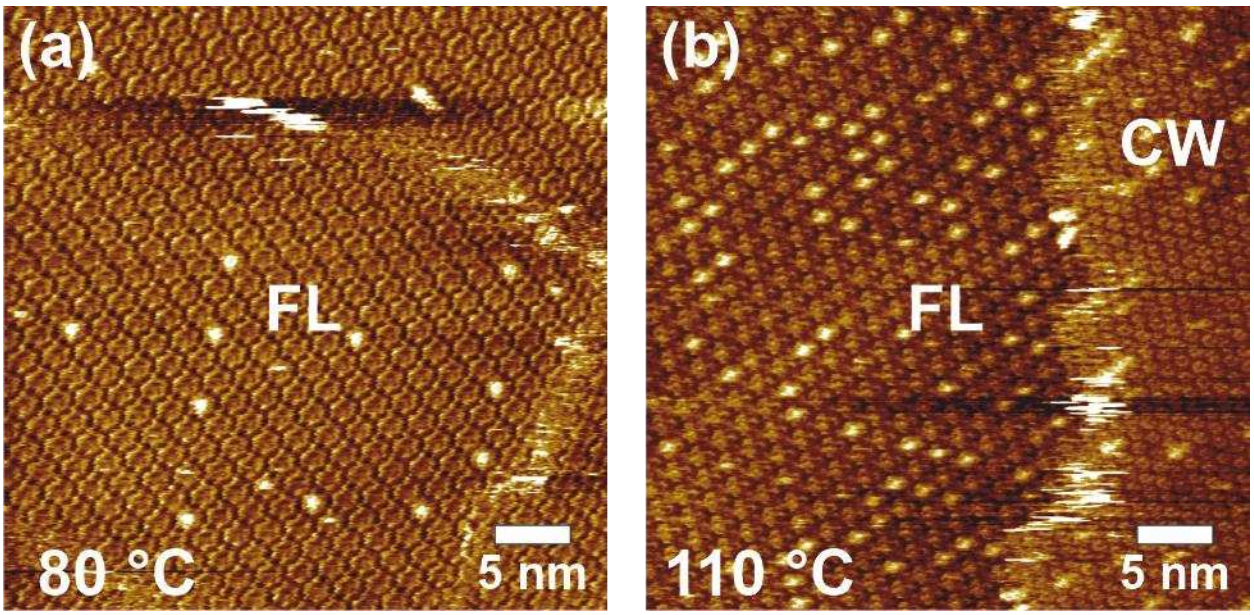

Figure 3. STM images of TMA monolayers on graphite(0001) acquired in saturated 6A solution after consecutive heating from room temperature to (a) 80 °C and (b) 110 °C. At a sample temperature of 80 °C we exclusively observed the flower polymorph (FL), whereas domains of the chickenwire (CW) polymorph emerged at 110 °C (see right hand side of (b)). Even though the contrast in these STM images can be uncommon, both polymorphs can be easily and unambiguously distinguished by the vast difference in lattice parameters. (sample voltages (a)

+0.53 V; (b) +0.51 V; setpoint currents were in the order of 30-50 pA, but precise values cannot be stated here due to the superposition with a temperature dependent offset current).

We first studied the stability of the flower polymorph in 6A for increasing temperature. A representative STM image acquired after heating from room temperature up to 80 °C is presented in Figure 3(a). Full coverage of the flower polymorph is maintained at this relatively high temperature, indicating a remarkable overall stability. Even after further increasing the temperature to 110 °C TMA monolayers still remained stable. Yet, as shown in Figure 3(b), we observed the co-existence of chickenwire and flower domains. In a subsequent STM experiment after cooling down to room temperature again, we exclusively observed the flower polymorph, indicating the back conversion of the chickenwire domains. This finding is in qualitative agreement with the theoretically predicted TMA phase diagram,[42] where the chickenwire polymorph constitutes the high-temperature phase, due to the reduced entropy cost associated with its lower molecular packing density. Hence, this reversible phase transition at around 100 °C provides evidence for superior thermodynamical stability of the flower polymorph in 6A at lower temperatures.

In variable temperature experiments with 6A solution we always observed few pores of the TMA polymorphs with bright appearance as also evident in Figure 3. This STM contrast indicates filling with an unknown, but fairly defined guest species. Moreover, we also noticed the development of an offset to the tunneling current that further increased with increasing temperature, and persisted after cooling down again to room temperature. We tentatively attribute both observations to heating related chemical changes of the TMA solution. A conceivable reaction would be anhydride formation between solute and solvent molecules, where either one or more carboxylic groups of TMA become extended by alkane tails or 6A-6A

anhydride dimers are formed. According to this hypothesis, the filled pores result from stable adsorption of the anhydride species, and the offset current is related to the water released by the condensation reaction. DFT structure optimization followed by Molecular Dynamics simulations of various anhydride species indicate their stable adsorption in the larger TMA pores with reasonably strong binding energies to account for the unknown species in STM images (cf. Supporting Information).

In a second series of experiments we addressed the question whether the less stable chickenwire can be converted into the flower polymorph in 6A. To prepare samples with a metastable chickenwire polymorph at the 6A-graphite interface, we first applied a small droplet of saturated TMA in 7A solution onto graphite in order to cover the entire surface with the chickenwire polymorph. Next, an excess of saturated TMA in 6A solution was applied to this sample. Subsequent STM imaging at room temperature exclusively showed the flower polymorph (cf. Supporting Information). The immediate spontaneous conversion of the pre-assembled chickenwire to the flower polymorph in 6A not only corroborates superior thermodynamical stability of the latter, but also demonstrates the absence of kinetic trapping at room temperature, even in these strongly H-bonded monolayers.

In addition, we explored the concentration dependence of TMA self-assembly for 6A and 7A solutions. Yet, we could not find any indications for a concentration-induced polymorphism. As anticipated, self-assembly of stable TMA monolayers was not observable anymore by STM below critical concentrations that were determined as $(0.42 \pm 0.06)\ \frac{mmol}{L}$ for 6A and $(0.40 \pm 0.02)\ \frac{mmol}{L}$ for 7A, respectively. These findings neither confirm nor contradict thermodynamic control.

Solvent Co-Adsorption

On the one hand, we found unambiguous experimental evidence for superior thermodynamical stability of the flower polymorph in 6A. On the other hand, according to our assessment of Δh and Δs, this cannot be explained by a primary solvent effect. To resolve this apparent contradiction, we propose solvent co-adsorption as a recognized important additional stabilizing or even structure-determining contribution for monolayer self-assembly at liquid-solid interfaces.[17, 32, 56-57] Intriguingly, both TMA polymorphs are porous, while the chickenwire is "more porous" than the flower polymorph on account of the molecular packing densities. Even though both polymorphs feature one large circular 1.0 nm wide pore in each unit cell, the chickenwire polymorph exhibits an approximately 2.5 times higher area density of these pores as compared to the flower polymorph owing to its smaller unit cell area (2.35 nm² for flower *versus* 5.85 nm² for chickenwire). Consequently, any thermodynamically favorable contribution from solvent co-adsorption in the larger pores would stabilize the chickenwire rather than the flower polymorph. Hence, stabilization of the flower polymorph by solvent co-adsorption must be related to its unique smaller and more elongated pores (orange ovals in Figure 1). Based on the seemingly good geometric match of extended (all trans) 6A solvent molecules with the smaller pores of the flower polymorph we propose that stereochemically specific solvent co-adsorption in these pores tilts the thermodynamic balance. According to this hypothesis, the additional thermodynamic stabilization is no longer feasible for 7A or longer chain fatty acids, simply because their dimensions exceed the pore size.

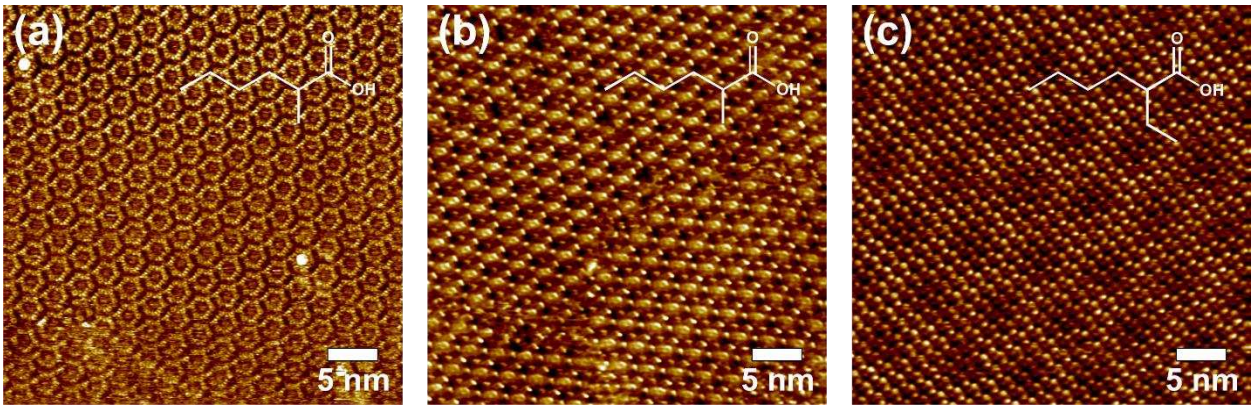

Figure 4. STM images of TMA monolayers on graphite(0001) acquired in saturated solutions using (a) / (b) methyl-6A and (c) ethyl-6A as solvent. Overlays show chemical structures of respective solvents. While methyl-6A still results in the flower polymorph, the chickenwire polymorph is observed in ethyl-6A. (sample voltages and current setpoints: (a) -582 mV, 61 pA; (b) -582 mV, 54 pA; (c) -571 mV, 54 pA).

To corroborate our hypothesis, we conducted experiments with side-substituted 6A solvents. The underlying idea is to evaluate polymorph selection for cases where the proposed solvent co-adsorption becomes sterically hindered, while the overall solvent characteristics is preserved. To avoid interferences with the monolayer H-bonding, the side groups should not form strong H-bonds. For these reasons, we further explored 2-methylhexanoic acid (methyl-6A) and 2-ethylhexanoic acid (ethyl-6A) as solvents (cf. Figure 4). We reckon that a significant contribution to the stabilization of 6A co-adsorption arises from H-bonds involving the solvent's carboxylic acid groups. Hence, we anticipate steric hindrance to be most effective when the side groups are in close proximity to the head group. Experimental results obtained for TMA saturated solutions are presented in Figure 4. Using methyl-6A as solvent still results in the flower polymorph, confirming a behavior analogous to unsubstituted 6A. It is worth to note that the intuitive contrast of the flower polymorph with bright appearing TMA molecules (see Figure

4(a)) was an exception, whereas an inverted contrast where both types of pores appeared brighter (see Figure 4(b)) was commonly observed. This holds also true for unsubstituted 6A (cf. Supporting Information) and may hint toward solvent co-adsorption in both type of pores of the flower polymorph. In contrast, further experiments using ethyl-6A as solvent indeed resulted in self-assembly of the chickenwire polymorph (cf. Figure 4(c)) in accord with our working hypothesis. The characteristic Moiré pattern indicates equivalency of the chickenwire polymorph in ethyl-6A and the typical 7A or 9A solvents. We conclude that steric hindrance imposed by ethyl side-group inhibits solvent co-adsorption in the smaller pores of the flower polymorph. As a consequence, the flower polymorph is thermodynamically less stable in ethyl-6A, resulting in self-assembly of the then thermodynamically favored chickenwire polymorph. These results support our hypothesis that the flower polymorph is eventually stabilized against the chickenwire polymorph by co-adsorption of solvent molecules in its smaller pores.

Summary and Conclusion

We present a comprehensive study of solvent-induced polymorphism in TMA monolayer self-assembly at fatty acid-graphite interfaces. This phenomenon is inherently more complex than concentration-induced polymorphism, because exchanging the solvent can have profound effects on the enthalpy gain, while varying solute concentrations primarily, if not exclusively, affects the entropy cost in a predictable manner. To provide a thermodynamical explanation, we evaluated Δg. The enthalpy gain per unit area Δh was quantified for both polymorphs in all three solvents with the aid of a Born-Haber cycle constructed from the measured TMA sublimation and dissolution enthalpies as well as DFT-calculated monolayer binding energies. The results indicate a slight enthalpic preference of the chickenwire polymorph in all solvents, but the differences in Δh are too small to be conclusive. Yet, the entropy cost per unit area Δs is

significantly larger for the flower than for the chickenwire polymorph owing to the 20% higher molecular packing density of the former. From this we conclude on the superior thermodynamic stability of the chickenwire polymorph in all solvents. Complementary variable temperature experiments in 6A solution unveiled a reversible phase transition from flower to chickenwire polymorph for increasing temperatures. With further support from the observed spontaneous conversion of the metastable chickenwire into the thermodynamically more stable flower polymorph in 6A already at room temperature, a kinetic stabilization of the flower polymorph in 6A can be ruled out. To explain the solvent-induced polymorphism of TMA on thermodynamic grounds, we propose a stabilizing contribution from the stereochemically specific solvent co-adsorption in the unique smaller elongated pores of the flower polymorph. This was corroborated by experiments with side-substituted 6A solvents, where sufficiently large steric hindrance resulted in self-assembly of the chickenwire polymorph.

The present study exemplifies a case of thermodynamical stabilization of a distinct monolayer polymorph by solvent co-adsorption, which is extremely sensitive to the solvent's molecular structure with a sharp threshold: Addition of just one methylene unit either in the main chain (7A instead of 6A) or in the side chain (ethyl-6A instead of methyl-6A) sterically hinders solvent co-adsorption in the smaller pores of the flower polymorph. These results demonstrate that polymorph specific solvent co-adsorption is particularly relevant when the molecular structure of the solvent becomes comparable to pore sizes and shapes. Extending these studies to further literature reported systems whose polymorphs exhibit differently sized and shaped pores would be desirable for concluding on the generality of this stabilizing mechanism.

Overwhelming and unambiguous results indicate a far more important and active role of solvents rather than just being a supply medium and background continuum. Solvent-induced

polymorphism in interfacial monolayers constitutes an ideal study object and versatile model system to promote the thermodynamical and molecular level understanding of solvent effects: STM facilitates a straightforward structural characterization, including the possibility to even directly image immobilized solvent molecules. Moreover, the temperature evolution of supramolecular systems can be directly studied by variable temperature STM experiments, where *in-situ* imaging at elevated temperatures allows capturing of reversible phase transitions. These remain unnoticed in *ex-situ* heating experiments, but serve as strong indicators for thermodynamic control. Lastly, solvent effects are anticipated to be particularly pronounced in monolayers as they are fully solvent exposed. In addition to STM imaging, monolayer self-assembly can be further explored by quantifying its thermodynamics or by the systematic variation of solvents. The thermodynamic analysis applied here based on the Born-Haber cycle and dissolution entropies is widely applicable and appropriate to unveil primary solvent effects. To explore further possible origins of solvent-induced polymorphism, it would be rewarding to also extend these studies to different classes of solvents, for instance non-protic solvents and solvents that exhibit inferior interaction with graphite as 1,2,4-tricholorbenzene or phenyloctane. To complement the thermodynamic analysis, structural variations of solvents that do not affect the main modes of interaction, for instance side-substitution of widely used alkanoic solvents, are invaluable for identifying and understanding solvent effects at the molecular level. The combined application of these two complementary approaches to prevalent cases of solvent-induced polymorphism, for instance of halogen or van der Waals bonded monolayers, holds great promise to enhance and deepen the understanding of ubiquitous solvent effects. Eventually, this can bring us one step closer to the holy grail of a priori structure prediction.

Material and methods

Experimental details

Room temperature and variable temperate STM experiments were carried out with home-built instruments. Details of the variable temperature instrument are described elsewhere.[55] Highly Oriented Pyrolytic Graphite (grade ZYB, Optigraph GmbH) samples were cleaved with adhesive tape prior to each experiment and mechanically cut PtIr (20/80) tips were used for imaging. TMA and fatty acid solvents were acquired from commercial sources (TCI and Sigma Aldrich) and used as received. The TMA sublimation enthalpy and the TMA dissolution enthalpies in 6A, 7A, and 9A were determined as described in our previous work.[43] Absorbance spectra were calibrated by comparison with solutions of known concentration for each respective solvent.

Computational details

Calculations of TMA adsorption on graphite were carried out using DFT, as implemented in the CP2K software.[58] The van der Waals density functional (vdW-DF) by Dion et al. was used,[59] with Goedecker-Teter-Hutter pseudopotentials,[60] and double-zeta valence polarized basis sets.[61] The Brillouin zone was sampled only at the Γ point. The graphite surface was modelled using periodic cells, with dimensions chosen such as to be commensurate with the experimentally measured size of the TMA chickenwire and flower polymorphs: a $\begin{pmatrix} 14 & 1 \\ -1 & 13 \end{pmatrix}$ graphene supercell, which is commensurate with (2×2) cells of the TMA chickenwire polymorph (8 TMA molecules), and a $\begin{pmatrix} 11 & 1 \\ -1 & 10 \end{pmatrix}$ graphene supercell, which is commensurate with one unit cell of the TMA flower polymorph (6 TMA molecules). Two layers of graphene were used to represent the graphite surface. The bottom layer was fixed and the top layer was allowed to optimize. The vertical cell dimension was 20 Å, which results in ~13 Å of vacuum between cells

in the vertical dimension. To calculate intermolecular binding energies, isolated (not adsorbed) TMA monolayers were similarly modelled as two-dimensional periodic systems, with a cell height of 20 Å in the vertical dimension. Ab-initio MD calculations of guest species in pores of the TMA network on graphene used the same DFT method and were performed with the NVT ensemble, time step 1 fs, run time 1 ps.

ASSOCIATED CONTENT

The following files are available free of charge.

sublimation enthalpy measurements of TMA, UV-Vis absorption spectra of TMA, additional STM images, calculations of guest adsorption (PDF)

AUTHOR INFORMATION

Corresponding Author

*Email: markus@lackinger.org

Author Contributions

The manuscript was written through contributions of all authors. All authors have given approval to the final version of the manuscript.

Funding Sources

Deutsche Forschungsgemeinschaft (DFG) through the Nanosystems-Initiative-Munich (NIM) cluster of excellence

ACKNOWLEDGMENT

Financial and ideal support by the Helmut Fischer Stiftung and the use of the THOMAS high-performance cluster which is partially funded by EPSRC (EP/P020194) and was accessed *via* N.M.'s membership of the UK's HEC Materials Chemistry Consortium (funded by EPSRC EP/L000202) are gratefully acknowledged.

ABBREVIATIONS

TMA, trimesic acid; DFT density functional theory; ISTM, Immersion Scanning Tunneling Microscope; STM Scanning Tunneling microscopy, ethyl-6A, 2-ethylhexanoic acid; methyl-6A, 2-methylhexanoic acid ;6A, hexanoic acid; 7A heptanoic acid; 9A nonanoic acid;

REFERENCES

1. Etter, M. C., Encoding and Decoding Hydrogen-Bond Patterns of Organic-Compounds. *Accounts Chem. Res.* **1990,** *23* (4), 120-126.
2. Lackinger, M.; Heckl, W. M., Carboxylic Acids: Versatile Building Blocks and Mediators for Two-Dimensional Supramolecular Self-Assembly. *Langmuir* **2009,** *25* (19), 11307-11321.
3. De Feyter, S.; De Schryver, F. C., Self-assembly at the liquid/solid interface: STM reveals. *J. Phys. Chem. B* **2005,** *109* (10), 4290-4302.
4. Kampschulte, L.; Lackinger, M.; Maier, A. K.; Kishore, R. S. K.; Griessl, S.; Schmittel, M.; Heckl, W. M., Solvent induced polymorphism in supramolecular 1,3,5-benzenetribenzoic acid monolayers. *J. Phys. Chem. B* **2006,** *110* (22), 10829-10836.
5. Shao, X.; Luo, X. C.; Hu, X. Q.; Wu, K., Solvent effect on self-assembled structures of 3,8-bis-hexadecyloxy-benzo[c]cinnoline on highly oriented pyrolytic graphite. *J. Phys. Chem. B* **2006,** *110* (3), 1288-1293.
6. Mamdouh, W.; Uji-i, H.; Ladislaw, J. S.; Dulcey, A. E.; Percec, V.; De Schryver, F. C.; De Feyter, S., Solvent controlled self-assembly at the liquid-solid interface revealed by STM. *J. Am. Chem. Soc.* **2006,** *128* (1), 317-325.
7. Li, Y. B.; Ma, Z.; Qi, G. C.; Yang, Y. L.; Zeng, Q. D.; Fan, X. L.; Wang, C.; Huang, W., Solvent effects on supramolecular networks formed by racemic star-shaped oligofluorene studied by scanning tunneling microscopy. *J. Phys. Chem. C* **2008,** *112* (23), 8649-8653.
8. Takami, T.; Mazur, U.; Hipps, K. W., Solvent-Induced Variations in Surface Structure of a 2,9,16,23-Tetra-tert-butyl-phthalocyanine on Graphite. *J. Phys. Chem. C* **2009,** *113* (40), 17479-17483.
9. Zhang, X.; Chen, Q.; Deng, G. J.; Fan, Q. H.; Wan, L. J., Structural Diversity of a Monodendron Molecule Self-Assembly in Different Solvents Investigated by Scanning Tunneling Microscopy: From Dispersant to Counterpart. *J. Phys. Chem. C* **2009,** *113* (36), 16193-16198.

10. Liu, J.; Zhang, X.; Yan, H. J.; Wang, D.; Wang, J. Y.; Pei, J.; Wan, L. J., Solvent-Controlled 2D Host-Guest (2,7,12-Trihexyloxytruxene/Coronene) Molecular Nanostructures at Organic Liquid/Solid Interface Investigated by Scanning Tunneling Microscopy. *Langmuir* **2010,** *26* (11), 8195-8200.
11. Xu, L.; Miao, X. R.; Zha, B.; Deng, W. L., Self-Assembly Polymorphism: Solvent-Responsive Two-Dimensional Morphologies of 2,7-Ditridecyloxy-9-fluorenone by Scanning Tunneling Microscopy. *J. Phys. Chem. C* **2012,** *116* (30), 16014-16022.
12. Silly, F., Selecting Two-Dimensional Halogen Halogen-Bonded Self-Assembled 1,3,5-Tris(4-iodophenyl)benzene Porous Nanoarchitectures at the Solid-Liquid Interface. *J Phys Chem C* **2013,** *117* (39), 20244-20249.
13. Wu, Y. C.; Li, J. X.; Yuan, Y. L.; Dong, M. Q.; Zha, B.; Miao, X. R.; Hu, Y.; Deng, W. L., Halogen bonding versus hydrogen bonding induced 2D self-assembled nanostructures at the liquid-solid interface revealed by STM. *Phys. Chem. Chem. Phys.* **2017,** *19* (4), 3143-3150.
14. Fu, C.; Orgiu, E.; Perepichka, D. F., Face-on vs. edge-on: tuning the structure of tetrathiafulvalene monolayers with solvent. *J. Mater. Chem. C* **2018,** *6* (14), 3787-3791.
15. Lei, S.; Tahara, K.; De Schryver, F. C.; Van der Auweraer, M.; Tobe, Y.; De Feyter, S., One Building Block, Two Different Supramolecular Surface-Confined Patterns: Concentration in Control at the Solid–Liquid Interface. *Angew. Chem. Int. Ed.* **2008,** *47*, 2964 –2968.
16. Blunt, M. O.; Adisoejoso, J.; Tahara, K.; Katayama, K.; Van der Auweraer, M.; Tobe, Y.; De Feyter, S., Temperature-Induced Structural Phase Transitions in a Two-Dimensional Self-Assembled Network. *J. Am. Chem. Soc.* **2013,** *135* (32), 12068-12075.
17. Gutzler, R.; Sirtl, T.; Dienstmaier, J. F.; Mahata, K.; Heckl, W. M.; Schmittel, M.; Lackinger, M., Reversible Phase Transitions in Self-Assembled Monolayers at the Liquid-Solid Interface: Temperature-Controlled Opening and Closing of Nanopores. *J. Am. Chem. Soc.* **2010,** *132* (14), 5084-5090.
18. Ciesielski, A.; Szabelski, P. J.; Rzysko, W.; Cadeddu, A.; Cook, T. R.; Stang, P. J.; Samori, P., Concentration-Dependent Supramolecular Engineering of Hydrogen-Bonded Nanostructures at Surfaces: Predicting Self-Assembly in 2D. *J. Am. Chem. Soc.* **2013,** *135* (18), 6942-6950.
19. Adisoejoso, J.; Tahara, K.; Lei, S. B.; Szabelski, P.; Rzysko, W.; Inukai, K.; Blunt, M. O.; Tobe, Y.; De Feyter, S., One Building Block, Two Different Nanoporous Self-Assembled Mono layers: A Combined STM and Monte Carlo Study. *ACS Nano* **2012,** *6* (1), 897-903.
20. Mazur, U.; Hipps, K. W., Kinetic and thermodynamic processes of organic species at the solution-solid interface: the view through an STM. *Chem. Commun.* **2015,** *51* (23), 4737-4749.
21. Gutzler, R.; Cardenas, L.; Rosei, F., Kinetics and thermodynamics in surface-confined molecular self-assembly. *Chem. Sci.* **2011,** *2* (12), 2290-2300.
22. Dienstmaier, J. F.; Mahata, K.; Walch, H.; Heckl, W. M.; Schmittel, M.; Lackinger, M., On the Scalability of Supramolecular Networks - High Packing Density vs. Optimized Hydrogen Bonds in Tricarboxylic Acid Monolayers. *Langmuir* **2010,** *26* (13), 10708-10716.
23. Ishikawa, Y.; Ohira, A.; Sakata, M.; Hirayama, C.; Kunitake, M., A two-dimensional molecular network structure of trimesic acid prepared by adsorption-induced self-organization. *Chem. Commun.* **2002,** (22), 2652-2653.
24. Dmitriev, A.; Lin, N.; Weckesser, J.; Barth, J. V.; Kern, K., Supramolecular Assemblies of Trimesic Acid on a Cu(100) Surface. *J. Phys. Chem. B* **2002,** *106*, 6907-6912.
25. Su, G. J.; Zhang, H. M.; Wan, L. J.; Bai, C. L.; Wandlowski, T., Potential-induced phase transition of trimesic acid adlayer on Au(111). *J. Phys. Chem. B* **2004,** *108* (6), 1931-1937.

26. Lackinger, M.; Griessl, S.; Heckl, W. M.; Hietschold, M.; Flynn, G. W., Self-assembly of trimesic acid at the liquid-solid interface - a study of solvent-induced polymorphism. *Langmuir* **2005,** *21* (11), 4984-4988.
27. Li, Z.; Han, B.; Wan, L. J.; Wandlowski, T., Supramolecular nanostructures of 1,3,5-benzene-tricarboxylic acid at electrified au(111)/0.05 M H2SO4 interfaces: An in situ scanning tunneling microscopy study. *Langmuir* **2005,** *21* (15), 6915-6928.
28. Sheerin, G.; Cafolla, A. A., Self-assembled structures of trimesic acid on the Ag/Si(111)-(root 3 x root 3)R30 degrees surface. *Surf. Sci.* **2005,** *577* (2-3), 211-219.
29. Nath, K. G.; Ivasenko, O.; Miwa, J. A.; Dang, H.; Wuest, J. D.; Nanci, A.; Perepichka, D. F.; Rosei, F., Rational modulation of the periodicity in linear hydrogen-bonded assemblies of trimesic acid on surfaces. *J. Am. Chem. Soc.* **2006,** *128* (13), 4212-4213.
30. MacLeod, J. M.; Ivasenko, O.; Perepichka, D. F.; Rosei, F., Stabilization of exotic minority phases in a multicomponent self-assembled molecular network. *Nanotechnology* **2007,** *18* (42), -.
31. Ye, Y. C.; Sun, W.; Wang, Y. F.; Shao, X.; Xu, X. G.; Cheng, F.; Li, J. L.; Wu, K., A unified model: Self-assembly of trimesic acid on gold. *J. Phys. Chem. C* **2007,** *111* (28), 10138-10141.
32. Kampschulte, L.; Werblowsky, T. L.; Kishore, R. S. K.; Schmittel, M.; Heckl, W. M.; Lackinger, M., Thermodynamical equilibrium of binary supramolecular networks at the liquid-solid interface. *J. Am. Chem. Soc.* **2008,** *130* (26), 8502-8507.
33. Ha, N. T. N.; Gopakumar, T. G.; Gutzler, R.; Lackinger, M.; Tang, H.; Hietschold, M., Influence of Solvophobic Effects on Self-Assembly of Trimesic Acid at the Liquid-Solid Interface. *J. Phys. Chem. C* **2010,** *114* (8), 3531-3536.
34. Eder, G.; Kloft, S.; Martsinovich, N.; Mahata, K.; Schmittel, M.; Heckl, W. M.; Lackinger, M., Incorporation Dynamics of Molecular Guests into Two-Dimensional Supramolecular Host Networks at the Liquid–Solid Interface. *Langmuir* **2011,** *27* (22), 13563–13571.
35. Iancu, V.; Braun, K. F.; Schouteden, K.; Van Haesendonck, C., Probing the Electronic Properties of Trimesic Acid Nanoporous Networks on Au(111). *Langmuir* **2013,** *29* (37), 11593-11599.
36. Zheng, Q. N.; Liu, X. H.; Liu, X. R.; Chen, T.; Yan, H. J.; Zhong, Y. W.; Wang, D.; Wan, L. J., Bilayer Molecular Assembly at a Solid/Liquid Interface as Triggered by a Mild Electric Field. *Angew. Chem. Int. Ed.* **2014,** *53* (49), 13395-13399.
37. MacLeod, J. M.; Lipton-Duffin, J. A.; Cui, D.; De Feyter, S.; Rosei, F., Substrate Effects in the Supramolecular Assembly of 1,3,5-Benzene Tricarboxylic Acid on Graphite and Graphene. *Langmuir* **2015,** *31* (25), 7016-7024.
38. MacLeod, J. M.; Lipton-Duffin, J.; Fu, C. Y.; Taerum, T.; Perepichka, D. F.; Rosei, F., A 2D Substitutional Solid Solution through Hydrogen Bonding of Molecular Building Blocks. *ACS Nano* **2017,** *11* (9), 8901-8909.
39. Spitzer, S.; Helmle, O.; Ochs, O.; Horsley, J.; Martsinovich, N.; Heckl, W. M.; Lackinger, M., What can be inferred from moire patterns? A case study of trimesic acid monolayers on graphite. *Faraday Discuss.* **2017,** *204*, 331-348.
40. Lipton-Duffin, J.; Abyazisani, M.; MacLeod, J., Periodic and nonperiodic chiral self-assembled networks from 1,3,5-benzenetricarboxylic acid on Ag(111). *Chem. Commun.* **2018,** *54* (60).

41. Ubink, J.; Enache, M.; Stohr, M., Bias-induced conformational switching of supramolecular networks of trimesic acid at the solid-liquid interface. *J. Chem. Phys.* **2018,** *148* (17).
42. Conti, S.; Cecchini, M., Predicting molecular self-assembly at surfaces: a statistical thermodynamics and modeling approach. *Phys. Chem. Chem. Phys.* **2016,** *18* (46), 31480-31493.
43. Song, W. T.; Martsinovich, N.; Heckl, W. M.; Lackinger, M., Born-Haber Cycle for Monolayer Self-Assembly at the Liquid-Solid Interface: Assessing the Enthalpic Driving Force. *J. Am. Chem. Soc.* **2013,** *135* (39), 14854-14862.
44. Acree, W.; Chickos, J. S., Phase Transition Enthalpy Measurements of Organic and Organometallic Compounds. Sublimation, Vaporization and Fusion Enthalpies From 1880 to 2015. Part 1. C-1-C-10. *J. Phys. Chem. Ref. Data* **2016,** *45* (3).
45. Shayeganfar, F.; Rochefort, A., Electronic Properties of Self-Assembled Trimesic Acid Monolayer on Graphene. *Langmuir* **2014,** *30* (32), 9707-9716.
46. Martsinovich, N.; Troisi, A., Modeling the Self-Assembly of Benzenedicarboxylic Acids Using Monte Carlo and Molecular Dynamics Simulations. *J. Phys. Chem. C* **2010,** *114* (10), 4376-4388.
47. Song, W.; Martsinovich, N.; Heckl, W. M.; Lackinger, M., Thermodynamics of 4,4 '-stilbenedicarboxylic acid monolayer self-assembly at the nonanoic acid-graphite interface. *Phys. Chem. Chem. Phys.* **2014,** *16* (26), 13239-13247.
48. Marie, C.; Silly, F.; Tortech, L.; Mullen, K.; Fichou, D., Tuning the Packing Density of 2D Supramolecular Self-Assemblies at the Solid-Liquid Interface Using Variable Temperature. *ACS Nano* **2010,** *4* (3), 1288-1292.
49. Ahn, S.; Matzger, A. J., Six Different Assemblies from One Building Block: Two-Dimensional Crystallization of an Amide Amphiphile. *J. Am. Chem. Soc.* **2010,** *132* (32), 11364-11371.
50. Sirtl, T.; Song, W. T.; Eder, G.; Neogi, S.; Schmittel, M.; Heckl, W. M.; Lackinger, M., Solvent-Dependent Stabilization of Metastable Monolayer Polymorphs at the Liquid-Solid Interface. *ACS Nano* **2013,** *7* (8), 6711-6718.
51. Bhattarai, A.; Mazur, U.; Hipps, K. W., A Single Molecule Level Study of the Temperature-Dependent Kinetics for the Formation of Metal Porphyrin Monolayers on Au(111) from Solution. *J. Am. Chem. Soc.* **2014,** *136* (5), 2142-2148.
52. Jahanbekam, A.; Chilukuri, B.; Mazur, U.; Hipps, K. W., Kinetically Trapped Two-Component Self-Assembled Adlayer. *J. Phys. Chem. C* **2015,** *119* (45), 25364-25376.
53. Sirtl, T.; Song, W.; Eder, G.; Neogi, S.; Schmittel, M.; Heckl, W. M.; Lackinger, M., Solvent-Dependent Stabilization of Metastable Monolayer Polymorphs at the Liquid–Solid Interface. *ACS Nano* **2013,** *7* (8), 6711-6718.
54. English, W. A.; Hipps, K. W., Stability of a surface adlayer at elevated temperature: Coronene and heptanoic acid on Au(111). *J. Phys. Chem. C* **2008,** *112* (6), 2026-2031.
55. Ochs, O.; Heckl, W. M.; Lackinger, M., Immersion-scanning-tunneling-microscope for long-term variable-temperature experiments at liquid-solid interfaces. *Rev Sci Instrum* **2018,** *89* (5).
56. Yang, Y.; Wang, C., Solvent effects on two-dimensional molecular self-assmblies investigated by using scanning tunneling microscopy. *Curr. Opin. Colloid In.* **2009,** *14* (2), 135-147.
57. Jäckel, F.; Ai, M.; Wu, J. S.; Müllen, K.; Rabe, J. P., Solvent molecules in an epitaxially grown scaffold of star-shaped nanographenes. *J. Am. Chem. Soc.* **2005,** *127* (42), 14580-14581.

58. VandeVondele, J.; Krack, M.; Mohamed, F.; Parrinello, M.; Chassaing, T.; Hutter, J., QUICKSTEP: Fast and accurate density functional calculations using a mixed Gaussian and plane waves approach. *Comput. Phys. Commun.* **2005,** *167* (2), 103-128.
59. Dion, M.; Rydberg, H.; Schröder, E.; Langreth, D. C.; Lundqvist, B. I., Van der Waals density functional for general geometries. *Phys. Rev. Lett.* **2004,** *92* (24).
60. Goedecker, S.; Teter, M.; Hutter, J., Separable dual-space Gaussian pseudopotentials. *Phys Rev B* **1996,** *54* (3), 1703-1710.
61. VandeVondele, J.; Hutter, J., Gaussian basis sets for accurate calculations on molecular systems in gas and condensed phases. *J. Chem. Phys.* **2007,** *127* (11).

TOC graphic: